ChemComm

Accepted Manuscript

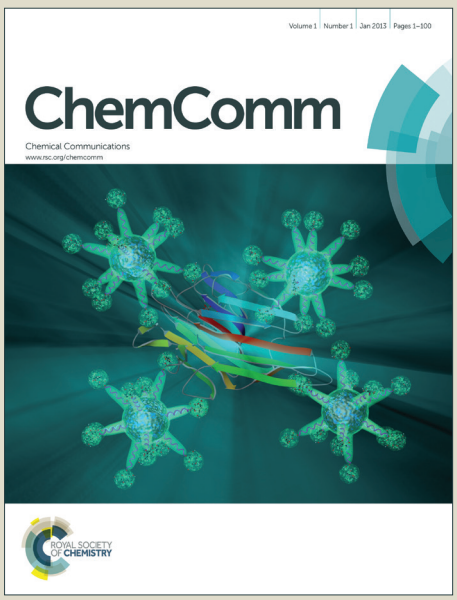

ROYAL SOCIETY OF CHEMISTRY

www.rsc.org/chemcomm

Chemical Communications

RSCPublishing

COMMUNICATION

What Does the Sr-Substituted 2.1 Å Resolution Crystal Structure of Photosystem II Reveal About the Water Oxidation Mechanism?

Cite this: DOI: 10.1039/xoxxoooooox

Received ooth January 2012,
Accepted ooth January 2012

DOI: 10.1039/xoxxoooooox

www.rsc.org/

Richard Terrett,[a] Simon Petrie,[a] Ron J. Pace[a] and Rob Stranger[a,b*]

A density functional study of the Sr-substituted Photosystem II water oxidising complex demonstrates that its recent X-ray crystal structure is consistent with a $(Mn^{III})_4$ oxidation state pattern, and with a Sr-bound hydroxide ion. The Sr-water/hydroxide interactions rationalize differences in the exchange rates of substrate water and kinetics of dioxygen bond formation relative to the Ca-containing structure.

Photosystem II in green plants and algae, is responsible for oxidising water to molecular oxygen. This occurs within a Mn_4Ca catalytic metal cluster known as the water oxidising complex (WOC). During the four-electron oxidation process, the WOC cycles through several intermediate states, S_0… S_4, of increasingly higher mean oxidation level.[1] However, both the mechanism of water oxidation and the metal oxidation levels throughout the S states, remain contentious.

Over the past decade, X-ray crystal structures of Photosystem II (PS II) have appeared at progressively improved resolution, from 3.5 to 2.9 Å.[2] These structures, presumed to represent the photosystem in the dark stable S_1 state, have revealed considerable detail concerning the Water Oxidising Complex (WOC) in PS II, in particular, the positions of the metal atoms and their coordination. In 2011, Umena et al.[3] published an X-ray structure of PS II at 1.9 Å, the first at atomic resolution, which clearly resolved the positions of the Mn and Ca atoms in the WOC, the oxo-bridges connecting the metal atoms and a number of coordinated waters (**Figure 1**).

Nevertheless, certain aspects of the the 1.9 Å structure have been controversial.[4] The long Mn1–Mn2 and Mn2–Mn3 distances (2.8 and 2.9 Å, respectively) conflict with those derived from high-precision EXAFS measurements[5] and earlier lower-resolution X-ray structures[2c-e] of PS II. The Mn EXAFS data for the functional WOC in the S_1 and S_2 states indicate the presence of two Mn–Mn vectors of ~2.70 Å and these are consistent with values of 2.65 and 2.70 Å reported for the Mn1–Mn2 and Mn2–Mn3 distances in the earlier 3.0/2.9 Å resolution XRD structures.[2d,e] This discrepancy has prompted suggestions that the 1.9 Å structure is compromised by photo-reduction of the Mn centres during the data collection,[4a-d,6] possibly reduced to the S_{-3} state.[4d,e] However, the dosage levels used were at least 10 times less than those employed previously in XRD studies of PS II, resulting in no more than ~25% reduction to Mn^{II}.[7] Even more disconcerting is that the 2.9 Å structure, which was subject to much higher X-ray dosages, shows no significant perturbation of the Mn centres on the basis of the reported Mn–Mn distances. The other major concern in the 1.9 Å structure is the identity and position of the unusual O5 species (Figure 1) which weakly binds to four metals of the WOC, Mn1, Mn3, Mn4 and Ca, at distances between 2.4 and 2.7 Å. If O5 is an oxo or a hydroxide group, it is unlikely to be at such long distances from the metal centres, particularly if one or more Mn are in the IV oxidation state.

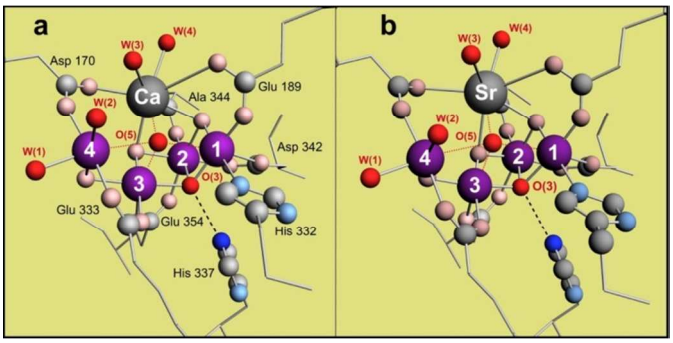

Figure 1. Diagram detailing the close correspondence between the WOC geometries of (a) Ca-containing and (b) Sr-containing PSII, as determined from the respective 1.9 Å resolution[3] and 2.1 Å resolution[13] XRD studies on these structures.

Recent computational studies[4] have addressed these anomalous features of the WOC in the 1.9 Å crystal structure, but were unable to reproduce the long Mn–Mn distances nor the unusual position of O5. Generally, these calculations assumed a mean oxidation level of +3.5 for the Mn centres in the S_1 state of the WOC. However, spectroscopic studies on the WOC do not preclude a mean Mn oxidation level of +3.0.[8] In particular, on the basis of the 'multiline' signal observed in the EPR spectrum of the S2 state of PS II, either a $(Mn^{IV})(Mn^{III})_3$ or $(Mn^{IV})_3(Mn^{III})$ oxidation state assignment is possible. We have labelled these alternatives as the 'Low Oxidation State' (LOS) and 'High Oxidation State' (HOS) paradigms, respectively. The HOS paradigm, with a $(Mn^{IV})_2(Mn^{III})_2$ oxidation

pattern for S_1, is favoured by most groups, largely on the basis of XANES and EPR evidence.[8a] However, we recently showed that when the metal ligand environments are properly accounted for, the XANES data are more consistent with the LOS paradigm for S_1, namely $(Mn^{III})(Mn^{IV})(Mn^{III})(Mn^{II})$.[9] Further analysis of other spectroscopic data (X-ray, UV-Vis, NIR) also support this conclusion.[8b,c] Finally, recent experimental studies by Dismukes et al.,[10] counting electrons removed from Mn^{II} ions during functional photo-assembly of PS II, validates the LOS paradigm for the WOC.

In light of the above, we recently undertook a computational study of the WOC in the 1.9 Å crystal structure assuming that the Mn oxidation levels conformed to the LOS paradigm.[11] Importantly, in the 1.9 Å structure, His337 is directly orientated towards the μ_3-oxo bridge (O3) and, as our earlier calculations revealed,[12a] is close enough to engage in H-bonding (**Figure 1**). Our modelling revealed a remarkable geometric change in the Mn_4Ca cluster, triggered by a proton transfer from a terminal water on Mn4 to the Nτ of His337. This allows His337 to engage in H-bonding with O3 which converts Mn2 from the IV to III oxidation state, thus lengthening the Mn1–Mn2 and Mn2–Mn3 bonds to around 2.9 Å, in good agreement with the crystal structure values. Deprotonation of a water on Mn4 favours the III oxidation state on this metal rather than II found in our earlier modelling of the 2.9 Å structure.[12] As a result, the sequence of Mn oxidation states change from (III)(IV)(III)(II) in the 2.9 Å structure to $(III)_4$ in the 1.9 Å structure. This change also resolved the identity of the O5 species which was found to be a water ligand, balanced at the intersection of the Jahn-Teller axes on Mn1, Mn3 and Mn4 and H-bonded to the now terminal hydroxide on Mn4 (**Figure 2a**). It successfully reproduced the long bonds between O5 and Mn1, Mn3, Mn4 and Ca in the 1.9 Å crystal structure.

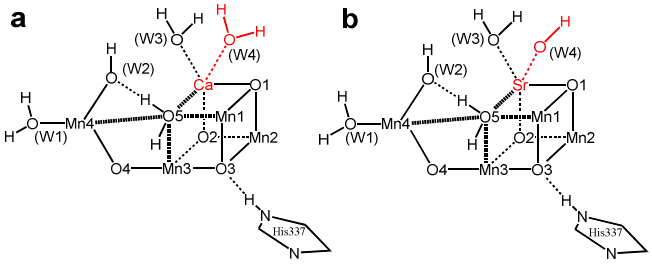

Figure 2. A comparison of our best-fit models to (a) the 1.9 Å resolution PSII WOC[3] and (b) the 2.1 Å resolution Sr-substituted WOC.[13] For simplicity, only the metal atoms, oxo bridges, metal-coordinated water ligands, and the His337 residue are shown. The Ca- and Sr-containing models are very similar, except for the identification of ligand W4 (highlighted in red) in the two structures.

Attempts by others[4] to rationalize O5 as either an oxo or hydroxo group in the HOS paradigm resulted in its strong binding to a Mn centre in the IV oxidation state, either Mn1 or Mn4. To resolve this, it was suggested[4j,k] that the unusual position of O5 results from a resonance process, with O5 inter-converting between an oxo group bound to Mn1 or Mn4. The Mn centre binding O5 is always in the IV state and the other Mn in the III state. If this resonance occurs in the OEC, then it should reflect in the electron density associated with O5. However, the WOC electron density in the 1.9 Å Ca structure shows that O5 is similar to the other oxo bridges, O1 to O4, in the metal cluster, suggesting that the resonance mechanism described above is unlikely.

Given that the low oxidation paradigm successfully rationalises the WOC geometries inferred by EXAFS and seen in the 2.9 and 1.9 Å crystal structures, without invoking radiation induced changes, we now consider the recent Sr-substituted 2.1 Å resolution crystal structure of PS II.[13] This structure exhibits a number of parallels with its Ca analogue - long Mn1–Mn2 and Mn2–Mn3 distances of 2.8 and 2.9 Å, respectively, and an anomalous O5 group weakly bound (2.4 to 2.7 Å) to four metals in the cluster (**Figure 1**). The His337 orientation and Nτ–O3 distance of approximately 3.0 Å suggests again that, analogous to the 1.9 Å Ca structure, His337 is undergoing H-bonding with the μ_3-oxo bridge. The fact that these features closely mimic those seen in the Ca structure would suggest that they are not an artefact of Mn photo-reduction.

To compare the two structures, we have undertaken DFT calculations,[14] assuming the LOS paradigm, on a model of the 2.1 Å Sr-substituted structure incorporating the Mn_4SrO_5 core, all coordinating amino acids (Asp170, Glu189, His332, Glu333, Asp342, Ala344, Glu354) constrained at their β-carbon positions using the X-ray structure coordinates, and bound water groups (W1…W4). Our model also included His337, Tyr161, His190, Gln165 and Arg357 as these residues H bond with W3, W4, O2 or O3. In addition, several non-coordinating crystallographic waters, in the vicinity of Sr, Tyr161 and His190, were incorporated due to their importance in the H-bonding network involving the WOC. Details of the computational model are elaborated upon in the Supporting Information.

The calculated metal–metal and selected metal–ligand distances for the antiferromagnetic (ABAB) coupling arrangement are listed in **Table 1** along with the reported values from the 2.1 Å crystal structure (averaged over monomers A and B). For comparison, the corresponding calculated and crystallographic values for the 1.9 Å Ca structure are also given. While the overall geometry of the WOC in the Sr-containing structure is very similar to the Ca structure, there are obvious differences. Firstly, the Sr atom has clearly moved outwards, away from the other three Mn ions in the Mn_3SrO_4 cubane, resulting in lengthening of all the Sr–Mn vectors relative to the Ca analogue by ~0.2 Å. This outward displacement of the Sr atom is also reproduced in the calculated structure with a similar increase of ~0.25 Å in the Sr–Mn vectors.

In contrast to the Ca/Sr-Mn distances, the differences between the reported Mn-Mn distances in the two crystal structures is much smaller, around 0.05 Å, and this is mostly consistent with the calculated values where an average difference of ~0.1 Å is seen. Similar to the Ca structure, the Sr structure exhibits long Mn1–Mn2 and Mn2–Mn3 distances of 2.78 and 2.93 Å. We were only able to reproduce these distances if H-bonding between His337 and O3 was invoked which ensured that the Mn oxidation pattern was $(III)_4$. Indeed, our calculations indicate that there is a propensity for His337 to transfer a proton to the O3 bridge. However, since the O3 protonated structures led to excessive expansion of the Mn1–Mn2 and Mn2–Mn3 distances to around 2.95 Å, subsequent calculations limited this interaction by constraining the N_{His337}–H distance to ~1.1 Å. As found in our modelling of the 1.9 Å Ca structure, in the absence of this H-bonding interaction, the Mn oxidation states adopt a (III)(IV)(III)(II) pattern and much shorter Mn1–Mn2 and Mn2–Mn3 distances are obtained.

Like the 1.9 Å Ca structure, the Sr structure possesses a weakly bound oxo group (O5) with long bonds, between 2.4 and 2.7 Å, to Mn1, Mn3, Mn4 and Sr. Our calculations show that this is only possible if two conditions are met. Firstly, O5 must be a water ligand and secondly, all the Mn centres must be in the III oxidation state which is only possible for the S_1 state of PS II in the LOS paradigm.

For the $(III)_4$ oxidation pattern, O5 sits approximately at the intersection of the Jahn-Teller axes on Mn1, Mn3 and Mn4, accounting for the long bonds to these metals between 2.8 and 3.4 Å.

Table 1. Comparison of key crystallographic and computed metal—metal and metal—ligand distances for the Sr-substituted WOC and the Ca-containing WOC.

Distance/Å	2.1 Å Sr Structure		1.9 Å Ca Structure	
	Expt[a]	Calc	Expt[b]	Calc
Mn1-Mn2	2.78	2.82	2.80	2.79
Mn2-Mn3	2.93	2.91	2.90	2.92
Mn3-Mn4	2.88	3.09	2.94	2.93
Mn1-Mn3	3.34	3.40	3.29	3.55
Mn1-Mn4	5.06	5.30	4.98	5.19
Sr/Ca-Mn1	3.56	3.77	3.48	3.56
Sr/Ca-Mn2	3.50	3.53	3.32	3.25
Sr/Ca-Mn3	3.64	3.86	3.43	3.62
Sr/Ca-Mn4	4.00	4.10	3.79	4.32
Sr/Ca-W3	2.64	2.62	2.40	2.54
Sr/Ca-W4	2.30	2.30	2.44	2.63
Mn1-O5	2.66	3.00	2.60	2.56
Mn3-O5	2.42	3.46	2.39	3.25
Mn4-O5	2.56	3.15	2.48	3.30
Sr/Ca-O5	2.59	2.90	2.64	2.50

a ref 13
b ref 3

In addition to the longer Sr–Mn distances relative to the Ca structure, the other noticeable difference concerns the water groups (W3, W4) bound to Sr. Whereas the Ca–W3 and Ca–W4 bonds in the 1.9 Å structure are similar, averaging 2.42 Å over monomers A and B, the corresponding distances in the Sr structure are significantly different, 2.64 and 2.30 Å, respectively (Table 1). On the basis of the long Sr–W3 bond, it was suggested that this water is activated in the structure and thus a likely candidate for one of the substrate waters in PS II.[13] Conversely, since the Sr–W4 bond was only 0.1 Å shorter than the Ca–W4 bond, it was presumed to be in a non-activated form.

Initial calculations on our model system with two waters bound to Sr revealed that the calculated Sr–W3 bond was in good agreement with the observed crystallographic distance of 2.69 Å but the calculated Sr–W4 bond of 2.76 Å was almost 0.5 Å too long. Inclusion of hydrogen bonding partners Tyr161 and Gln165 reduces this distance to 2.49 Å. This prompted additional calculations where W4 was modelled as a hydroxide group rather than water (**Figure 2b**), and returned Sr–W3 and Sr–W4 bond lengths of 2.62 and 2.30 Å, respectively, in excellent agreement with the crystal structure values (**Figure 3**). These distances, particularly Sr–W4, are quite dependent on the H-bonding network seen in Figure 3 involving W3, W4, Tyr161, His190, Gln165 and the nearby non-coordinating waters. When these additional residues are removed from the model, longer Sr–W3 and Sr–W4 distances are obtained. We find plausible stabilisation of the short Sr–W4 bond by coordination of W4 to either the phenolic oxygen of Tyr161 or the terminal amide oxygen of Gln165. Both orientations appear energetically competitive and elicit similarly good agreement of the Sr–W3 and –W4 distances with crystallographic data. The results strongly argue that W4 corresponds to a hydroxide and not a water ligand in the 2.1 Å Sr-substituted structure. Further, since our calculated Sr–W3 distance of 2.62 Å is very close to the reported crystal structure value, we conclude that this water is not in an activated form. However, on the basis of our earlier modelling,[11,12d,e] we consider that this ligand, and the O5 species, are likely to be the two substrate waters in PS II.

Isotope-exchange experiments using ^{18}O labelled water,[15] show that in Sr-substituted PS II, the exchange rate for the slowly exchanging water increases by a factor of ~4 (in all S states). This increase is totally consistent with the Sr–W3 bond being approx. 0.2 Å longer, and thus more weakly bound, than in the Ca structure. Furthermore, while our modelling strongly suggests that W4 is deprotonated and bound to Sr in the form of a hydroxide, it also reveals that W4 undergoes H-bonding with W3 and Tyr161. This H-bonding interaction may provide insight to understanding the reduction, by a factor of 3 – 10, in the oxygen-evolving activity of Sr-substituted PS II compared to Ca-based PS II,[16] as it is likely to impact on the ability of W3 to form an O–O bond with the other substrate water, O5, in the higher S states, and consequently, the oxygen-evolving activity of the WOC.

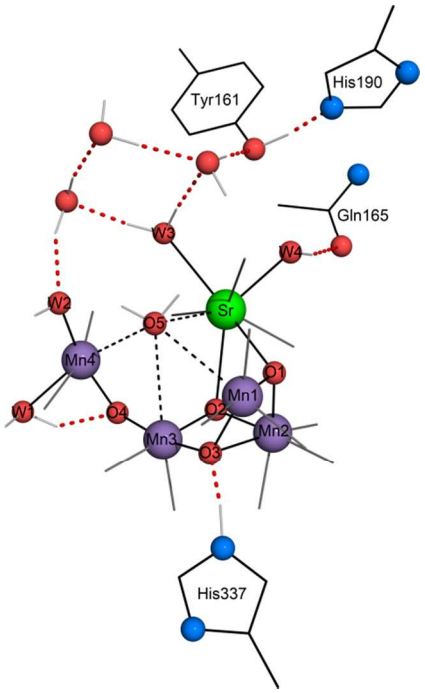

Figure 3. Calculated WOC structure showing H-bonding network connecting Sr with Tyr161, His190 and Gln165. Inclusion of these residues, and the associated H-bonding network, yields good agreement with the crystallographic Sr–W3 and Sr–W4 distances (see **Table 1**). For clarity, only metal atoms, oxo bridges, and water-ligand O atoms are shown explicitly.[17]

In conclusion, the recent 2.1 Å resolution Sr-substituted crystal structure of PS II reveals the same unusual features found in the 1.9 Å Ca structure, namely long Mn1–Mn2 and Mn2–Mn3 distances and the anomalous O5 group weakly bound to four metals, Mn1, Mn3, Mn4 and Sr, in the WOC. Our calculations show that these features can only be rationalized in the LOS paradigm in which the Mn centres adopt a $(III)_4$ oxidation pattern as a result of His337 undergoing H-bonding with the μ_3-oxo bridge, O3. The key structural difference between the Ca and Sr systems involves the W3 and W4 groups bound to the alkaline earth metal. On the basis of our calculations, the short Sr–W4 bond of approximately 2.3 Å is consistent with a hydroxide group and not a water as previously proposed.[13] The reported Sr–W3 bond of 2.62 Å is ~0.2 Å longer than the Ca–W3 bond. The weaker binding of W3 provides an obvious explanation for the observed faster exchange rate of the slow water in Sr-substituted PS II. Furthermore, the deprotonation of W4 in the Sr structure, and consequently its propensity to

undergo H-bonding with W3 and Tyr161, may also be responsible for the reduced oxygen-evolving activity observed for Sr-substituted PS II. This suggests that the deprotonation of W4 to a hydroxide is not just an artefact of the 2.1 Å Sr-substituted crystal structure but the preferred form of W4 in Sr-substituted PS II.

Considering the above points, an interesting picture emerges which highlights structural factors largely ignored in mechanistic considerations to date. These have focussed closely on the Mn cluster itself and oxygen groups directly ligating it, which are presumed to include the substrate moieties themselves.[8a] The fact that the principal geometric differences between the Ca and Sr crystal structures occur in the region containing the alkaline earth metal and its associated H bonding network to Tyr161 (rather than the Mn cluster per se), suggests the intimate involvement of this region with substrate water binding and O-O bond formation. In particular, it is strongly implied, consistent with our earlier proposals,[12] that at least one substrate water (slow exchanging) is directly bound to the alkaline earth metal throughout the S state cycle. Further, the rate limiting events in the O-O bond forming step, are likely to be directly influenced by the precise interaction of this water within a H-bonded chain proceeding to Tyr 161. This focus is quite different from other current mechanistic proposals.[4]

Notes and references

[a] Research School of Chemistry, College of Physical Sciences and Mathematics, The Australian National University, ACT 0200, Australia.
[b] Email: Rob.Stranger@anu.edu.au.

RS and RJP gratefully acknowledge financial assistance from the Australian Research Council, and the provision of supercomputing time on the platforms of the NCI (National Computational Infrastructure) Facility in Canberra, Australia.

1 K. Satoh, T. Wydrzynski, *Photosystem II: The Light Drive Water: Plastoquinone Oxidoreductase*, Springer, Dordrecht, The Netherlands, **2005**, 11-22.
2 a) A. Zouni, H.-T. Witt, J. Kern, P. Fromme, N. Krauss, W. Saenger and P. Orth, *Nature*, 2001, **409**, 739-743; b) N. Kamiya and J.-R. Shen, *Proc. Natl. Acad. Sci. USA*, 2003, **100**, 98-103; c) K. N. Ferreira, T. M. Iverson, K. Maghlaoui, J. Barber and S. Iwata, *Science*, 2004, **303**, 1831-1838; d) B. Loll, J. Kern, W. Saenger, A. Zouni and J. Biesiadka, *Nature*, 2005, **438**, 1040-1044; e) A. Guskov, J. Kern, A. Gabdulkhalov, M. Broser, A. Zouni and W. Saenger, *Nat. Struct. Mol. Biol*., 2009, **16**, 334-342.
3 Y. Umena, K. Kawakami, J.-R. Shen and N. Kamiya, *Nature*, 2011, **473**, 55-60.
4 a) S. Luber, I. Rivalta, Y. Umena, K. Kawakami, J.-R. Shen, N. Kamiya, G. W. Brudvig and V. Batista, *Biochem.*, 2011, **50**, 6308-6311; b) P. E. M. Siegbahn, *ChemPhysChem*, 2011, **12**, 3274-3280; c) W. Ames, D. A. Pantazis, V. Krewald, N. Cox, J. Messinger, W. Lubitz and F. Neese, *J. Am. Chem. Soc*., 2011, **133**, 19743-19757; d) A. Galstyan, A. Robertazzi and E. W. Knapp, *J. Am. Chem. Soc*., 2012, **134**, 7442-7449; e) A. Grundmeier and H. Dau, *Biochim. Biophys. Acta Bioenerg*., 2012, **1817**, 88-105; f) P. E. M. Siegbahn, *Phys. Chem. Chem. Phys*., 2012, **14**, 4849-4856; g) M. Kusunoki, *J. Photochem. Photobiol*., 2011, **104**, 100-110; h) T. Saito, S. Yamanaka, K. Kanda, H. Isobe, Y. Takano, Y. Shigeta, Y. Umena, K. Kawakami, J.-R. Shen, N. Kamiya, M. Okumura, M. Shoji, Y. Yoshioka and K. Yamaguchi, *Int. J. Quantum Chem*., 2012, **112**, 253-276; i) S. Yamanaka, T. Saito, K. Kanda, H. Isobe, Y. Umena, K. Kawakami, J.-R. Shen, N. Kamiya, M. Okumura, H. Nakamura and K. Yamaguchi, *Int. J. Quantum Chem*., 2012, **112**, 321-343; j) D. A. Pantazis, W. Ames, N. Cox, W. Lubitz and F. Neese, *Angew. Chem. Int. Ed. Engl*., 2012, **51**, 9935-9940; k) H. Isobe, M. Shoji, S. Yamanaka, Y. Umena, K. Kawakami, N. Kamiya, J.-R. Shen and K. Yamaguchi, *Dalton Trans*., 2012, **41**, 13727-13740.
5 a) M. Haumann, C. Müller, P. Liebisch, L. Iuzzolino, J. Dittmer, M. Grabolle, T. Neisius, W. Meyer-Klaucke and H. Dau, *Biochem.*, 2005, **44**, 1894-1908; b) J. Yano, Y. Pushkar, P. Glatzel, A. Lewis, K. Sauer, J. Messinger, U. Bergmann and V. Yachandra, *J. Am. Chem. Soc*., 2005, **127**, 14974-14975.
6 J. Yano, J. Kern, K.-D. Irrgang, M. J. Latimer, U. Bergmann, P. Glatzel, Y. Pushkar, J. Biesiadka, B. Loll, K. Sauer, J. Messinger, A. Zouni and V. K. Yachandra, *Proc. Natl. Acad. Sci. USA*, 2005, **102**, 12047-12052.
7 J. Vinyard, G. M. Ananyev and G. C. Dismukes, *Annu. Rev. Biochem*., 2013, **82**, 577-606.
8 a) P. Gatt, R. Stranger and R. J. Pace, *J. Photochem. Photobiol. B*, 2011, **104**, 80-93; b) R. J. Pace, Lu Jin and R. Stranger, *Dalton Trans*., 2012, **41**, 11145-11160; c) R. J. Pace, R. Stranger and S. Petrie, *Dalton Trans*., 2012, **41**, 7179-7189.
9 a) A. R. Jaszewski, R. Stranger and R. J. Pace, *Phys. Chem. Chem. Phys*., 2009, **11**, 5634-5642; b) A. R. Jaszewski, S. Petrie, R. J. Pace and R. Stranger, *Chem. Eur. J*., 2011, **17**, 5699-5713.
10 D. R. J. Kolling, N. Cox, G. M. Ananyev, R. J. Pace and G. C. Dismukes, *Biophys. J*., 2012, **103**, 313-322.
11 P. Gatt, S. Petrie, R. Stranger and R. J. Pace, *Angew. Chem. Int. Ed. Engl*., 2012, **51**, 12025-12028.
12 a) S. Petrie, P. Gatt, R. Stranger and R. J. Pace, *Chem. Phys. Phys. Chem*., 2012, **14**, 4651-4657; b) S. Petrie, P. Gatt, R. Stranger and R. J. Pace, *Phys. Chem. Chem. Phys*., 2012, **14**, 11333-11343; c) S. Petrie, R. Stranger, P. Gatt and R. J. Pace, *Chem. Eur. J*., 2007, **13**, 5082-5089; d) S. Petrie, R. Stranger and R. J. Pace, *Angew. Chem. Int. Ed. Engl*., 2010, **49**, 4233-4236; e) S. Petrie, R. Stranger and R. J. Pace, *Chem. Eur. J*., 2010, **16**, 14026-14042.
13 F. H. M. Koua, Y. Umena, K. Kawakami and J.-R. Shen, *Proc. Natl. Acad. Sci. USA*, 2013, **110**, 3889-3894.
14 a) *Amsterdam Density Functional v.2013.01*, S.C.M., Theoretical Chemistry, Vrije Universiteit, Amsterdam, the Netherlands, http://www.scm.com; b) Calculations were performed in an unrestricted fashion using the GGA Becke-Perdew density functional and the TZP all-electron basis set. Relativistic corrections using the Zeroth-Order Regular Approximation (ZORA) were applied to the strontium basis set.
15 G. Hendry and T. Wydrzynski, *Biochem.*, 2003, **42**, 6209-6217.
16 A. Boussac and A. W. Rutherford, *Biochem.*, 1988, **27**, 3476-3483; b) K. L. Westphal, N. Lydakis-Simantiris, R. I. Cukier, G. T. Babcock , *Biochem.,* **2000,** *39,* 16220-16229.
17 The PyMOL Molecular Graphics System, Version 1.6.x Schrödinger, LLC.

